Effects of nano-dust particles on heat transfer from multiple jets impinging on a flat plate

Amirhosein Hadipour[1] · Mehran Rajabi Zargarabadi[1] · Saman Rashidi[2]

Abstract

The present study aims to investigate the effects of dusty air on the behavior of flow and heat transfer due to a row of turbulent jets impinging on a flat plate for different values of jet-to-target plate distance. Hence, the impinging air with three dust concentrations of 0.32, 1.0, and 1.8 gr m^3 has been considered for the numerical simulations. The validations of numerical simulations have been performed for clean air impinging jets. A silicon heater is used to supply the uniform heat flux of 2000 W m^2 on the target plate. An IR camera is also used for measuring the local temperature over the surface. The values of Nusselt number under the low nozzle-to-target plate distance (H/D $\geq$ 1.0) are compared with those for high nozzle-to-target plate distance (H/D > 1.0) for the jet Reynolds numbers of 7000 and 15,000. Comparisons of the results indicate that the numerical data achieved by the RNG k-ε model show satisfactory agreement with the experimental data. In the present study, the new investigation has been performed on the impact of the nozzle distances on the velocity and temperature fields over the heated surface for low distances for both clean and dusty air. The results show that the Nusselt number of dusty air is higher than that for the clean air in both stagnation and wall jet regions. It was also found that for the jet Reynolds number of 7000 the air with a dust concentration of 1.8 gr/m^3 provides a higher averaged Nusselt number by 18%, 45.8% and 39.5% times more than the Nusselt numbers of clean air for the jet-to-surface distances (H/D) of 0.1, 0.5, and 2.0, respectively. The average Nusselt number increases significantly with decreasing the jet-to-surface distance in the range of H/D = 0.5 to 0.1.

List of symbols

Ts	Surface temperature (K)
Tjet	Jet temperature (K)
D	Nozzle diameter (m)
H	Nozzle-to-surface distance (m)
K	Air thermal conductivity (Wm^1·K)
Nu	Nusselt number
P	Distance between jets (m)
q''	Heat flux (W m^2)
Re	Reynolds number
U_{jet}	Jet velocity (ms^1)
X	Axial distance (m)
Z	Axial distance (m)
y^+	Dimensionless distance
p	Static pressure (Pa)
ρ	Density (kg m^3)
$\rho_{p\infty}$	Density of particulate and bulk air-particle (kg m^3)
$V_{p\infty}$	Volume flow rate
u, v, w	Velocity (m·s^{-1})
c_{mp}	Mass of particles
c_{vp}	Dust volume concentrations
k	Turbulent kinetic energy (m^2·s^{-2})

Greek symbols

ε	Emissivity
ϑ	Kinematic viscosity (m^2·s^{-1})
μ	Dynamic viscosity (Kg·m^{-1} s^{-1})
ρ	Density (kg·m^{-3})

✉ Mehran Rajabi Zargarabadi
rajabi@semnan.ac.ir

1 Faculty of Mechanical Engineering, Semnan University, P.O.B. 35131-191, Semnan, Iran

2 Department of Energy, Faculty of New Science and Technologies, Semnan University, Semnan, Iran

Introduction

Impinging jet is one of the most effective practical techniques used in many industrial applications and thermal treatments, including sheet-form materials e.g., cooling of

gas turbine components, drying of textiles, paper, photographic films, heating or cooling of sheets of metal, glass, coated papers, veneer, etc. In the past decades, many studies have been conducted on the effects of impinging jets on the flow and thermal characteristics. For example, Esmailpour et al. [1] investigated the entropy generation of pulsed impinging jet. Guo et al. [2] studied the axisymmetric wall jet development in the confined jet impingement. Hadipour et al. [3] studied the effects of a triangular guide rib on the flow and heat transfer of impingement jet on an asymmetric concave surface. Siddique et al. [4] investigated the heat transfer augmentation of flat target surface under air jet impingement for the varying heat flux boundary condition. Doranehgard et al. [5] investigated the natural-gas diffusion in oil-saturated tight porous media. Hadipour et al. [6] studied the effect of micro-pin characteristics heat transfer of jet impinging to the flat surface. Lytle and Webb [7] investigated the influence of jet-to-plate distance of impinging jet on the Nusselt number distribution at low nozzle-to-surface distances. They proposed a relation based on the jet-to-surface distance for the stagnation point of Nusselt number.

Norbert et al. [8] investigated the temperature and velocity distributions of impinging jet on a semi-confined cavity. The authors found that with a decrease in the jet-to-plate distance, the local Nusselt number increases in the impingement region. The impact of spent air removal on the heat transfer rate at low spacing between the target surface and impinging jet was studied by Singh and Ekkad [9]. They found that low jet-to-surface distance plays an important role in the spent air removal from the system.
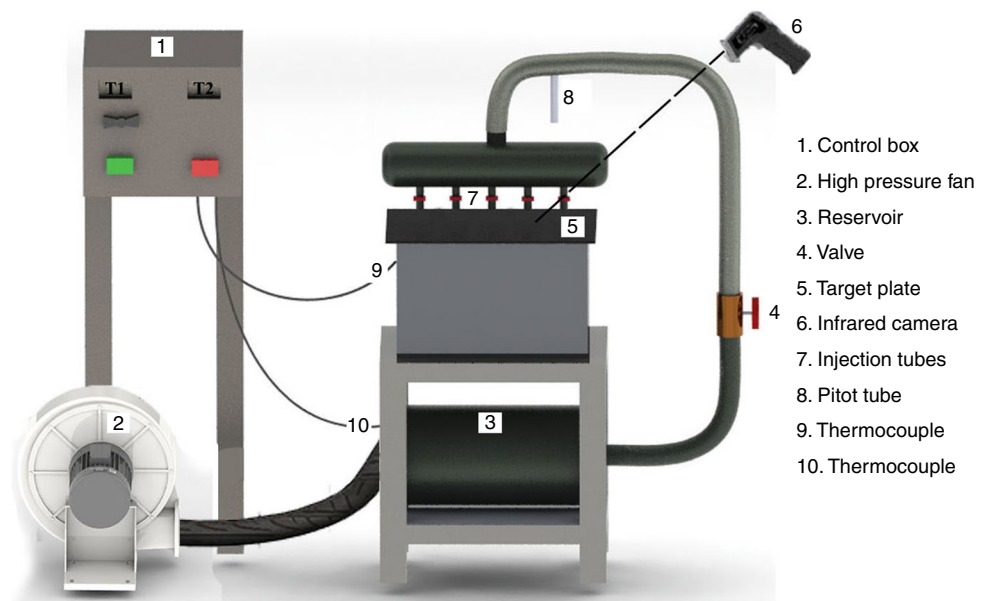
Grenson et al. [10] investigated the jet impingement with low jet-to-plate distances. Like previous experiments, they stated that for the low jet-to-surface distances, the distribution of local Nusselt number has a secondary maximum. Glaspell et al. [11] investigated the effect of water jet at small nozzle-to-surface distance on the heat transfer. They found that the stagnation Nusselt number can increase by decreasing the jet-to-plate distance. Choo and Kim [12] observed that for H/D ≥ 5, the features of adiabatic temperature are not contingent on the distance between the jet and target surface. Choo et al. [13] investigated the relation between the stagnation pressure and Nusselt number of the jet impingement for H/D in the range of 0.125 to 40. They observed that the local Nusselt number is dependent on the stagnation pressure. Greco et al. [14] found that the maximum heat transfer rate occurs at a low nozzle-to-plate distance. Zhu et al. [15] studied the transient heat transfer of impinging jet to flat surface at low distance between the jet and target plate. They found that at the low jet-to-jet distance, the heat transfer rate has the best performance. Hadipour and Rajabi [16] examined the temperature and velocity fields of jet impingement on a symmetrical concave surface at low nozzle-to-plate distance. They showed that the jets

with very small jet-to-plate distances provide better cooling efficiency. In an experimental investigation, Yu et al. [17] studied the impinging jet heat transfer with two rows of aligned jets.

Many studies have been focused on the impingement of row of jets on a surface. Fregeau et al. [18] examined the rate of heat transfer due to jet impingement for several values of jet-to-target surface distance. They used the Spalart–Allmaras turbulent model and observed the gratifying results for higher jet-to-target plate distances. The flow and heat transfer from the row jets impingement on a concave surface was studied by Craft et al. [19]. In their investigation, the k-ε model together with a wall function was used. They applied a standard wall function for the prediction of the Nusselt number. Sharif and Mothe [20] used various turbulent models for simulating the impinging jet on a concave plate. They observed that better efficiency can be achieved in reproducing the flow features by using the RSM models. Singh et al. [21] performed a numerical investigation on the heat transfer of circular impinging jet. They applied the different nozzle diameters and nozzle-to–target surface distances in their investigation. Their results showed that for all configurations at the impinging zone, all turbulent models over-estimate the Nusselt number. Fenot et al. [22, 23] performed an experimental investigation on a row of jet impingement to the concave and flat surfaces. They investigated the effects of geometric flow and flow parameters. They found that the influence of the near jets on the local Nusselt number is limited to a between jets area. On the other hand, the effectiveness greatly depends on the jet-to-jet distance. Whitaker et al. [24] examined the effects of particle size on the heat transfer due to jet impingement with the dusty air. They found that at high temperatures, air with particles with diameter larger than 10 microns has a higher heat transfer rate. Presley and Christensen [25] measured the thermal conductivity of dusty air. They mentioned that as the particle size of the dust increases, the thermal conductivity increases. Zhang et al. [26] focused on the dust concentration measurement technique based on ultrasonic changes. Their results indicated that the deviation between the experiments and theory is lower than 10% when the dust concentration is varied between 100 and 900 gr m^3. In this regard, Aliabadi et al. [27] also reported that using the 0.3% nanofluid flow can enhance the heat transfer coefficient effectively in cooling system.

According to the literature review, decreasing the nozzle-to-surface distance improves the rate of heat transfer and Nusselt number in whole of the target plate. It was found that there is no investigation due to a row jet impinging on a flat plate for low nozzle-to-surface distance for both clean and dusty air. As a result, the present study is focused on the impact of the nozzle distances on the velocity and temperature fields over the heated surface for low different distances.

Fig. 1 Experimental apparatus

1. Control box
2. High pressure fan
3. Reservoir
4. Valve
5. Target plate
6. Infrared camera
7. Injection tubes
8. Pitot tube
9. Thermocouple
10. Thermocouple

The effects of jet-to-plate distance in the range of 0.1 to 2 and the dust concentration in the range of 0 to 1.8 gr m^3 on the flow and heat transfer of row jets impinging have been investigated. Furthermore, the local Nusselt number and velocity distributions achieved by the experiments are compared with those obtained by the numerical simulation.

Experimental apparatus and methodologies

Experimental setup

The experimental equipment used in this study is shown in Fig. 1. This system contains the control box, a fan, flow controller valve, thermocouples, IR camera, and a flat surface under the electrical heat flux. The air in the nozzles is supplied by a high-pressure centrifugal fan. To ensure about the fully developed flow conditions at the jet exit, the length of the nozzle is assumed to be more than 20 times of the nozzle diameter.

Figures 2 and 3 show the target plate. The length (x-direction) and the width (z-direction) of this plate are 30 cm and 15 cm, respectively.

Test model

In this study, the cooling capacity of clean and dusty impinging jets over the flat plate has been evaluated. The test surface with 30*15*10 cm, shown in Figs. 2 and 3, is considered. The top surface is a steel plate with the thickness of 1 mm, which is heated with an electrical (silicone) heater. The jet diameter is 10 mm. In each experiment, first the heat flux of 2 kW.m^{-2} is provided and the jet velocity was
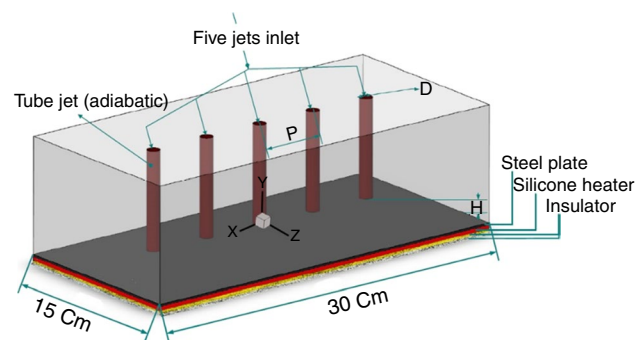

Fig. 2 Schematic of the impingement jet configuration
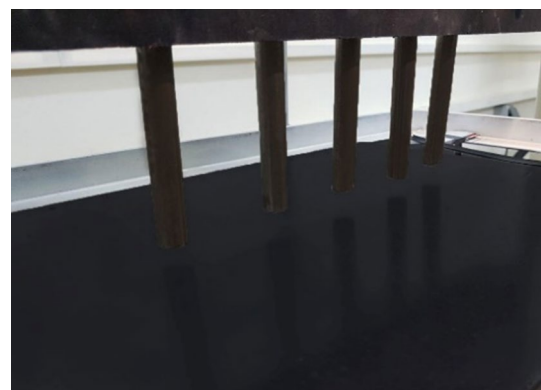

Fig. 3 Experimental facility

regulated by a calibrated hotwire anemometer. After reaching the steady-state condition, the target surface temperature is measured by an infrared camera. The local Nusselt number is defined by:

$$Nu = \frac{q''}{T_s - T_{jet}} \frac{D_{jet}}{k} \tag{1}$$

where D_{jet} is nozzle diameter (10 mm), T_s is target surface temperature and T_{jet} is air temperature at exit jet.

The velocity and temperature fields of the target plate are investigated for the Reynolds numbers of 7000 and 15,000. In addition, three jet-to-target distances of 0.1, 0.5, and 2 are tested. The jet Reynolds number is defined on the basis of the average output velocity of the nozzles and the nozzle diameter as follows:

$$Re = \frac{\rho U D_{jet}}{\mu} \tag{2}$$

where ρ is the density, u is the velocity of air at the nozzle exit, D_{jet} is the jet diameter, and μ is the dynamic viscosity of the air.

The total uncertainty comprises of many parameters, which affect the experiment in different ways [28]. Consider the value of M, which is dependent on variables x_1, x_2,..., x_N. The uncertainty of M is denoted by U and can be calculated from the following equation:

$$M = F(x_1, x_2, x_3, \dots x_n), \quad U^2(M) = \sum_{i=1}^{N} \left[\frac{\partial f}{\partial x_i}\right]^2 U^2(x_i) \tag{3}$$

where $U(x_i)$ is the uncertainty of variable xi. The local Nusselt number as a function of all parameters can be written as:
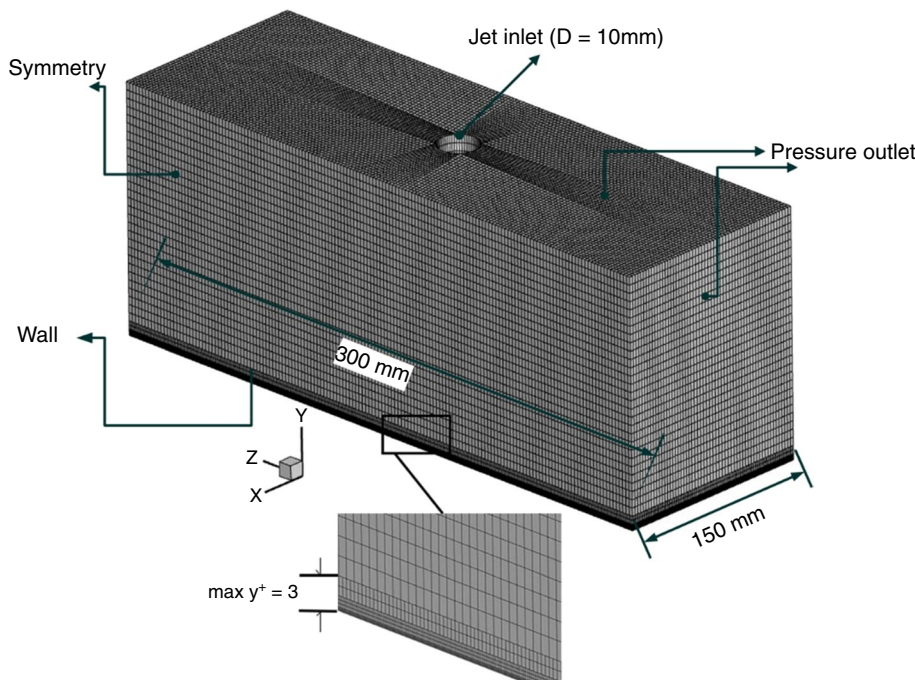
$$Nu = \frac{q''}{T_s - T_j} \frac{D_{jet}}{k} \quad Nu = F(q'', T_s, T_j) \tag{4}$$

By applying Eqs. (3) and (4), the uncertainty of local Nusselt number can be calculated by:

$$\begin{aligned}
U^2(NU) &= \left(\frac{\partial Nu}{\partial q''} U(q'')\right)^2 + \left(\frac{\partial Nu}{\partial T_s} U(T_s)\right)^2 + \left(\frac{\partial Nu}{\partial T_j} U(T_j)\right)^2 \\
&= \frac{D_{jet}}{k}\left[\left(\frac{1}{T_s - T_j} U(q'')\right)^2 + \left(\frac{q''}{(T_s - T_j)^2} U(T_s)\right)^2 + \left(\frac{q''}{(T_s - T_j)^2}(UT_j)\right)^2\right]
\end{aligned} \tag{5}$$

Fig. 4 Grid generated inside the computational domain

It is estimated that the averaged uncertainty values for Nusselt numbers is about $\pm 8.8\%$ through the Kline and McClintock method [28].

Numerical study

Geometry and boundary conditions

The boundary conditions and geometry of the present work are illustrated in Fig. 4. The computational domain consists of a single circular jet impinging on a flat plate. Three jet-to-surface distances are considered. On the target plate, the constant heat flux with the no-slip condition is used. The air with the standard conditions, temperature of 300 k, thermal conductivity of 0.26 w·mk[1], and viscosity of 1.78 kg·ms[1], is used. The air is considered as the Newtonian and incompressible-ideal-gas. The governing equations for simulating the present work are presented in the following section:

3.2 Governing equations

The transport equations in the present study can be expressed as:

$$\frac{\partial \left(\rho u_i \right)}{\partial x_i} = 0 \tag{6}$$

$$\frac{\partial}{\partial x_j} \left(\rho u_i u_j \right) = -\frac{\partial P}{\partial x_i} + \frac{\partial}{\partial x_j} \left(2\mu S_{ij} - \overline{\rho u_i' u_j'} \right) \tag{7}$$

$$\frac{\partial}{\partial x_j} \left(\rho C_P u_i T \right) = -\frac{\partial P}{\partial x_i} + \frac{\partial}{\partial x_j} \left(k \frac{\partial T}{\partial x_i} - \overline{\rho C_P u_i' T'} \right) \tag{8}$$

Recent studies have shown that the RNG k–ε model has better accuracy as compared with other turbulent models to predict hydrodynamic data in impinging jet flows over target surfaces with a higher convergence speed [3, 20]. The accuracy and high convergence speed of this model are due to some modifications including new constants and existence of an additional term on the right-hand side of the ε equation. It is noted that by using an appropriate mesh near the wall regions, all advantages of the RNG k–ε model can be achieved.

The RNG k–ε turbulent model is employed to simulate the flow and thermal fields [29]. In this model, the transport equations of k and ε are:

$$\rho u_j \frac{\partial}{\partial x_j} (k) = \frac{\partial}{\partial x_j} \left[\left(\mu + \frac{\mu_t}{\sigma_k} \right) \frac{\partial k}{\partial x_j} \right] + 2\mu_t S_{ij} S_{ji} - \rho \tag{9}$$

$$\rho u_j \frac{\partial}{\partial x_j} (\varepsilon) = \frac{\partial}{\partial x_j} \left[\left(\mu + \frac{\mu_t}{\sigma_\varepsilon} \right) \frac{\partial \varepsilon}{\partial x_j} \right] + C_{1\varepsilon} \frac{\varepsilon}{k} P_K - C_{2\varepsilon} \rho \frac{\varepsilon^2}{k} \tag{10}$$

where P_k can be calculated by:

$$P_K = \left[\mu_t \left(\frac{\partial U_i}{\partial x_j} \mu + \frac{\partial U_j}{\partial x_i} \right) - \frac{2}{3} \rho k \delta_{ij} \right] \frac{\partial U_i}{\partial x_j} \tag{11}$$

Theory of dust model

The previous studies showed that the particle size is varied in the range of 5 to 15 microns. $\rho_p = 2650 \left(kg\ m^{-3} \right), \gamma = 0.8 \left(N\ m^{-1} \right), \vartheta_{ARD} = 0.18, BFM = 2(\%)$ are the properties of the dust [24].

To achieve the mass flow rate of particles $\left(W_{p\infty} \right)$, the following equation can be used [30].

$$W_{p\infty} = c_{mp} \rho_{p\infty} \dot{V}_{p\infty} \tag{12}$$

The air-particle density can be expressed in the terms of the dust mass concentration c_{mp}. The dust volume concentration, c_{vp}, can be calculated by:

$$c_{mp} = \frac{1}{\rho_f / c_{vp} + \left(1 - \rho_f / \rho_p \right)} \tag{13}$$

For $\rho_f / \rho_p = 1$, the dust mass concentration is $c_{mp} = c_{vp} / \rho_f$. Since the air density, ρ_f, has the order of 100 Kg m^{-3}, the dust volume concentration can be expressed as follows [30]:

$$c_{mp} \approx \frac{c_{vp}}{\rho_f} \tag{14}$$

The chemical and physical properties of dusty air, applied in the present study, are presented in Table 1.

Table 1 Chemical and physical properties of dusty air [30, 32, 33]

| Properties of dusty air	Values	Units
Dust Concentration	1.8	g m^{-3}
Viscosity	1.52×10^{-5}	kg m^{-1} s^{-1}
Density of dust air	1.196	kg m^{-3}
Thermal conductivity (for volume filling factors 30%)	0.022	W m^{-1} K^{-1}
Mass-weighted specific heat capacity	756	J kg^{-1} K^{-1}
Mass-weighted mean density	2709	kg m^{-3}
Mass-weighted mean particle diameter	17.6	μm
Landing duration	20	s
Bulk melting temperature	1433	K
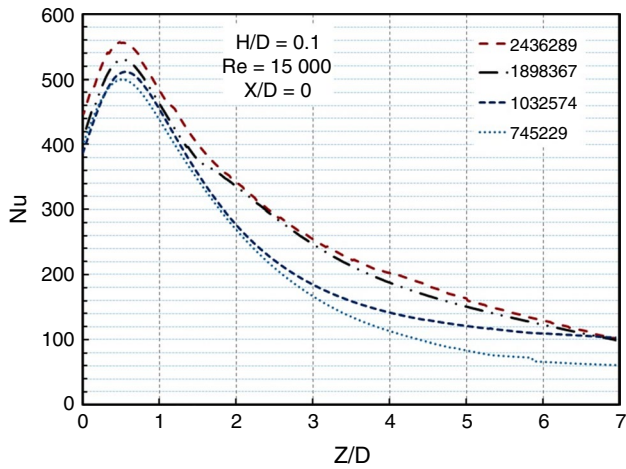
**Fig. 5** Results of grid independence test

Numerical procedure

In this study, the advection terms of transport equations have been discretized by the second-order scheme. The SIMPLEC algorithm has been adopted for the pressure–velocity coupling [31]. The absolute criteria for the convergence of mass conservation and momentum equations are less than 10^{-4} and they are lower than 10^{-7} for the energy equation.

Grid independence test

Figure 4 shows the structured grid generated inside the computational domain. To achieve the independency of the results from the grid sizes, different grids have been generated.

The grid test is performed for four grid numbers and the results are disclosed in Fig. 5. The Nusselt number is calculated at Re = 15,000 and X/D = 0. As shown in Fig. 5, the difference between the Nusselt numbers calculated by the grid

Fig. 6 Effect of the jet-to-surface distance on the local Nusselt number on the centerline plane (Z/D = 0) for **a** Re = 7000; **b** Re = 15,000
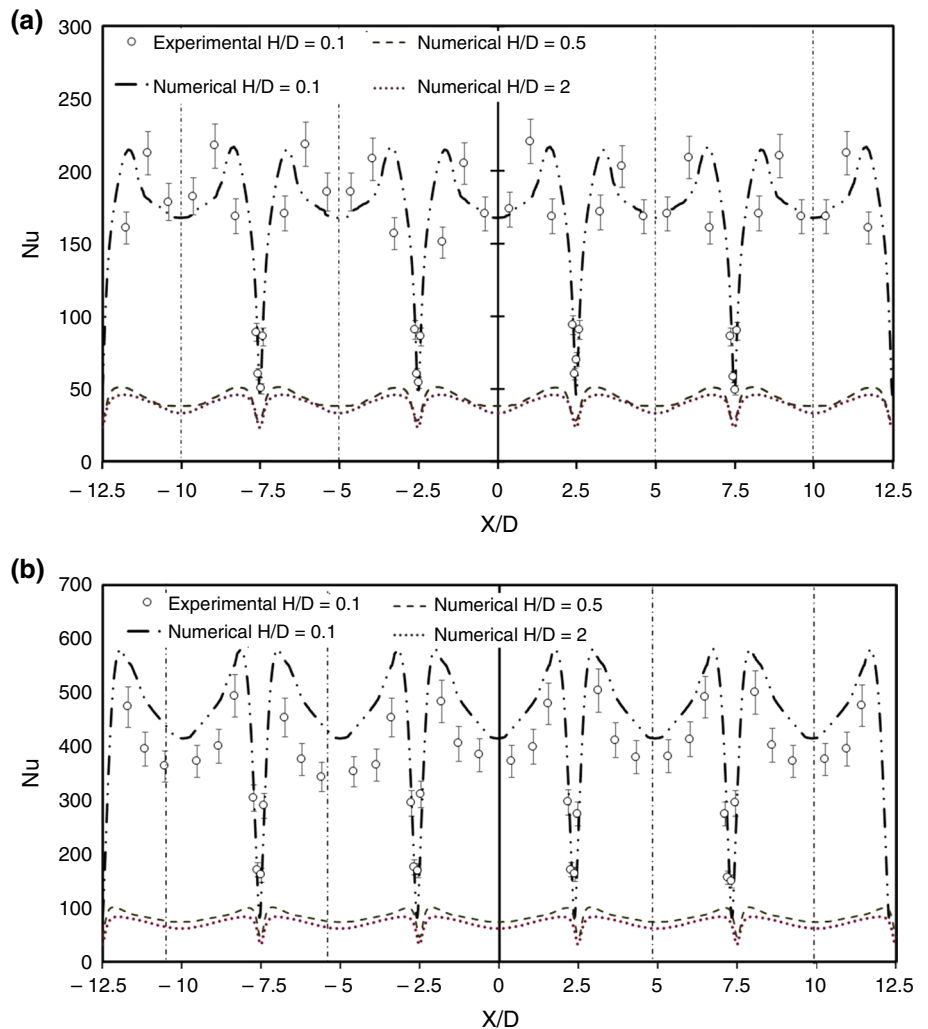
sizes of 1,898,367 and 2,436,289 are negligible. Hence, the grid number of 1,898,367 is used for the rest of simulations.

Results and discussion

In this work, the impact of jet-to-surface distance, jet-to-jet distance, and Reynolds number for dusty air at low jet-to-surface distance on the flow and thermal characteristics are investigated.

Thermal performance

Figure 6 illustrates the effects of the jet-to-surface distance on the local Nusselt number for two Reynolds numbers of 7000 and 15,000. Note that the local Nusselt number is plotted on the centerline plane (Z/D = 0) in this figure. The results confirm that reducing the jet-to-surface distance (H/D) from 2.0 to 0.1 leads to a significant increase in the local Nusselt number. When a row of jets is used in the jet impingement system, an area between the jets, called the dead area, is formed in which the value of Nusselt number is significantly decreased. This was also observed in the previous studies [19, 22, 23]. Figure 6 shows that by reducing the jet-to-surface distance (H/D) in the range of 2.0 to 0.5, a small increase in the local Nusselt number is achieved. However, as the H/D is decreased from 0.5 to 0.1, the local Nusselt number significantly increases. In other words, for the jet Reynolds number of 7000, the mean Nusselt number increases about 4.2% and the maximum value of Nusselt number increases about 9% as the jet-to-surface distance decreases from 2.0 to 0.5. The average Nusselt number and the maximum value of Nusselt number are increased about 186.7% and 328%, respectively, as the jet-to-plate distance is decreased in the range of 0.5 to 0.1. Both experimental and numerical results are shown in this figure for the

comparison. The good agreement between two results can be observed.

In general, the increase in the temperature between two jets can be described by the Nusselt number distribution in this area. Figure 7 exhibits the distributions of local Nusselt number on the middle line between the jets (X/D = 2.5) and centerline (X/D = 0) for the Reynolds number of 15,000 and different values of the jet to surface distance. The results show that by placing the nozzles at the lowest jet-to-target plate distance (e.g., H/D = 0.1), the Nusselt number at the region between the jets significantly decreases, while the Nusselt number distribution in the centerline is considerably increased in comparison with other jet-to-surface distances. Although for H/D = 0.1, the local Nusselt number significantly decreases in the dead fluid zone, but still in
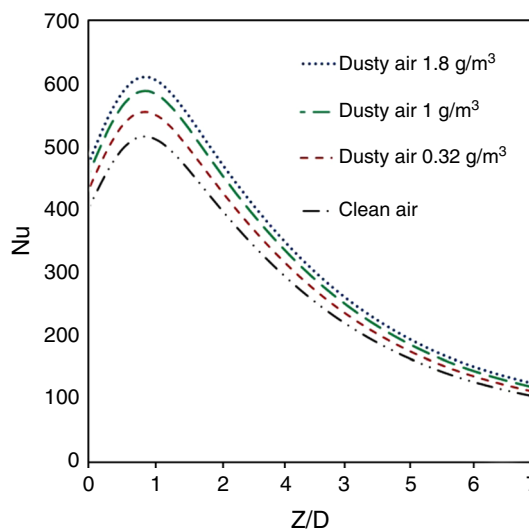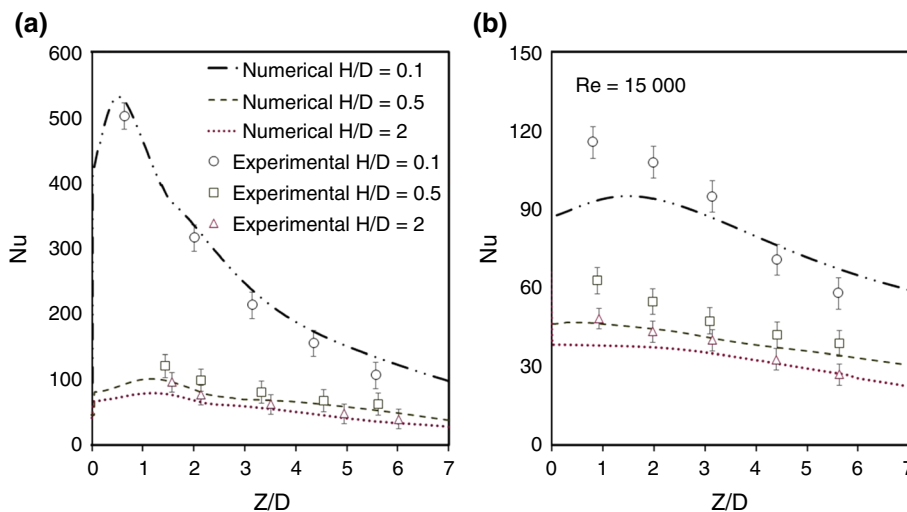
Fig. 8 Effect of air dust concentration on Nusselt number distribution at X/D = 0 for Re = 15,000, H/D = 0.1

Fig. 7 Nusselt number distribution for different values of H/D and Re = 15,000 on **a** centerline (X/D = 0); **b** line between two jets (X/D = 2.5)

comparison with other jet-to-surface distances, it has a considerable value in the region between the jets. The main reason for these changes of Nusselt number for the mentioned H/D in different areas of the target surface, is the difference in the flow of coolant fluid on the target surface. In this study, to better understand the reason for these changes of Nusselt number, the fluid flow on the target surface has been investigated.

Effect of air dust on Nusselt number distribution

In recent years, various studies focused on the impact of dust on heat transfer [24, 30, 32–35]. Most of these studies examined the effect of particle size and concentration of dust on the natural and forced heat convection. In this study, a new attempt was made to investigate the effect of dust on the jet impingement cooling system.
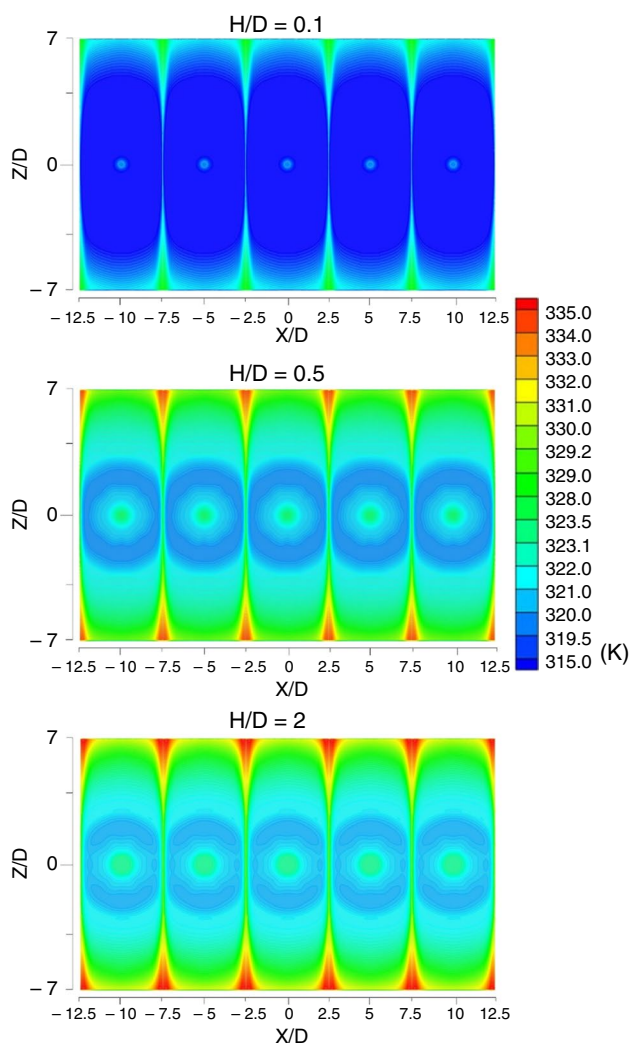
The effects of air dust on the Nusselt number distribution on centerline (X/D = 0) for Re = 15,000 are investigated in Fig. 8. Previous studies have shown that dust particles can greatly enhance the heat transfer process and adding dust to the air can increase the heat transfer coefficient [36, 37]. The results of this study show that the Nusselt number of dusty air is higher than that for the clean air in both stagnation and wall jet regions [38–40]. Also, by increasing the dust concentration from 0.32 g m^{-3} to 1.8 g m^{-3}, the local Nusselt number on throughout the target plate increases. It can be found that the impinging air with the dust concentration of 1.8 g m^{-3} can increase the maximum Nusselt number by 18% in comparison with that for the clean air jet.

The temperature distributions on the flat plate for different values of the jet-to-surface distance at the Reynolds number of 15,000 and the dust concentration of 0.32 g m^{-3} are disclosed in Fig. 9. It is observed that the temperature on the flat plate significantly decreases as the jet-to-surface distance is decreased from 2.0 to 0.1. As discussed earlier, due to the higher flow rate for the case of H/D = 0.1, the lower temperature values, varied in the range of 310 to 321 K, can
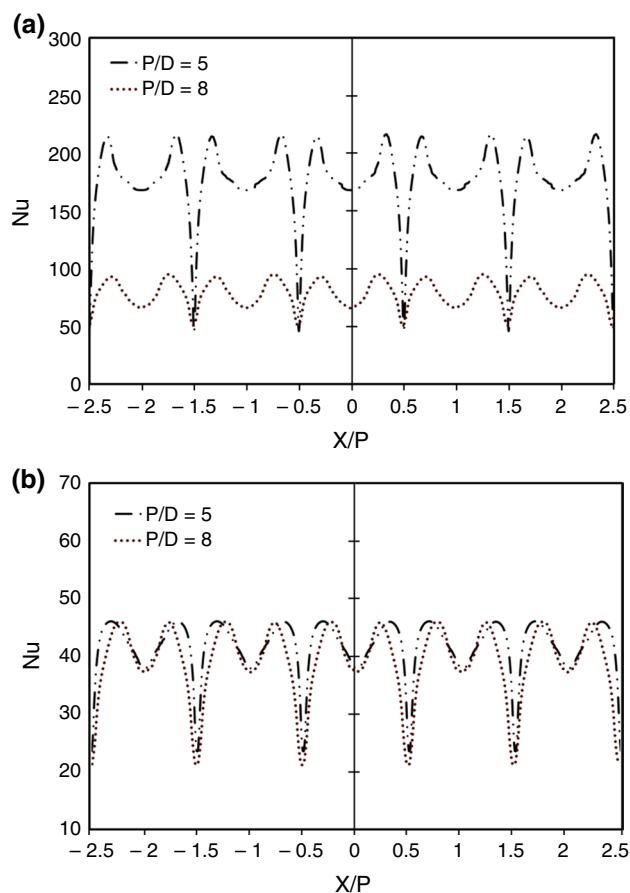

Fig. 9 Temperature contour at Re = 15,000 and dust concentration of 0.32 g/m3

Fig. 10 Effects of jet-to-jet distance on Nusselt number distribution at Re = 7000 and dust concentration of 0.32 g m^{-3} for **a** H/D = 0.1; **b** H/D = 2
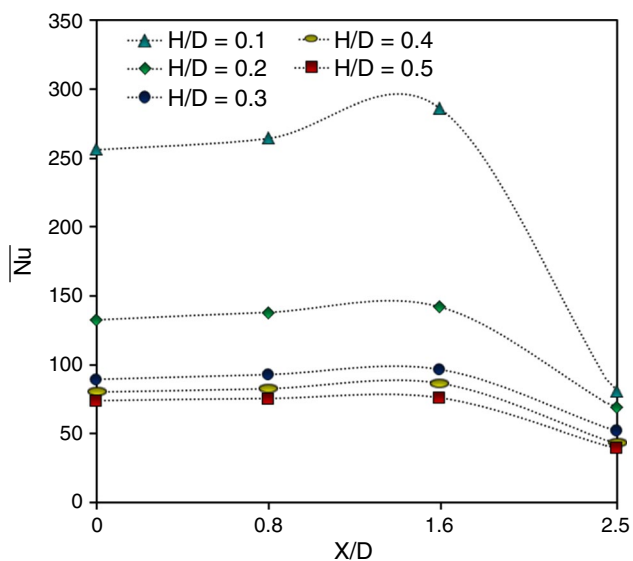
Fig. 11 Effect of jet-to-surface distance on average Nusselt number at dust concentration of 0.32 g m^{-3} at Re = 15,000

be achieved for this case. Note that the ranges of temperature variation for the cases of H/D = 0.5 and H/D = 2.0 are 318 to 333 K and 319 to 335 K, respectively.

Figure 10 shows the effect of jet-to-jet distance on the Nusselt number distribution for the Reynolds number of 7000, dust concentration of 0.32 g m^{-3}, and two values of jet-to-target plate distance (H/D = 0.1 and H/D = 2). It can be seen that by reducing the jet-to-jet distance, the Nusselt number increases. This trend is also observed in the previous studies conducted in this field [23, 41]. The previous studies showed that by reducing the jet-to-jet distance, the value of Nusselt number is increased but this increase is not significant [23, 41]. However, the results of this study show that by placing the nozzles at low nozzle-to-surface distance (e.g., H/D = 0.1), the value of Nusselt number significantly increases as the jet-to-jet distance is decreased. Figure 10 also shows that for the case of H/D = 2, the variations of jet-to-jet distance have low effects on the Nusselt number distribution, while the effects of these variations on the Nusselt number value are significant for the case of H/D = 0.1.

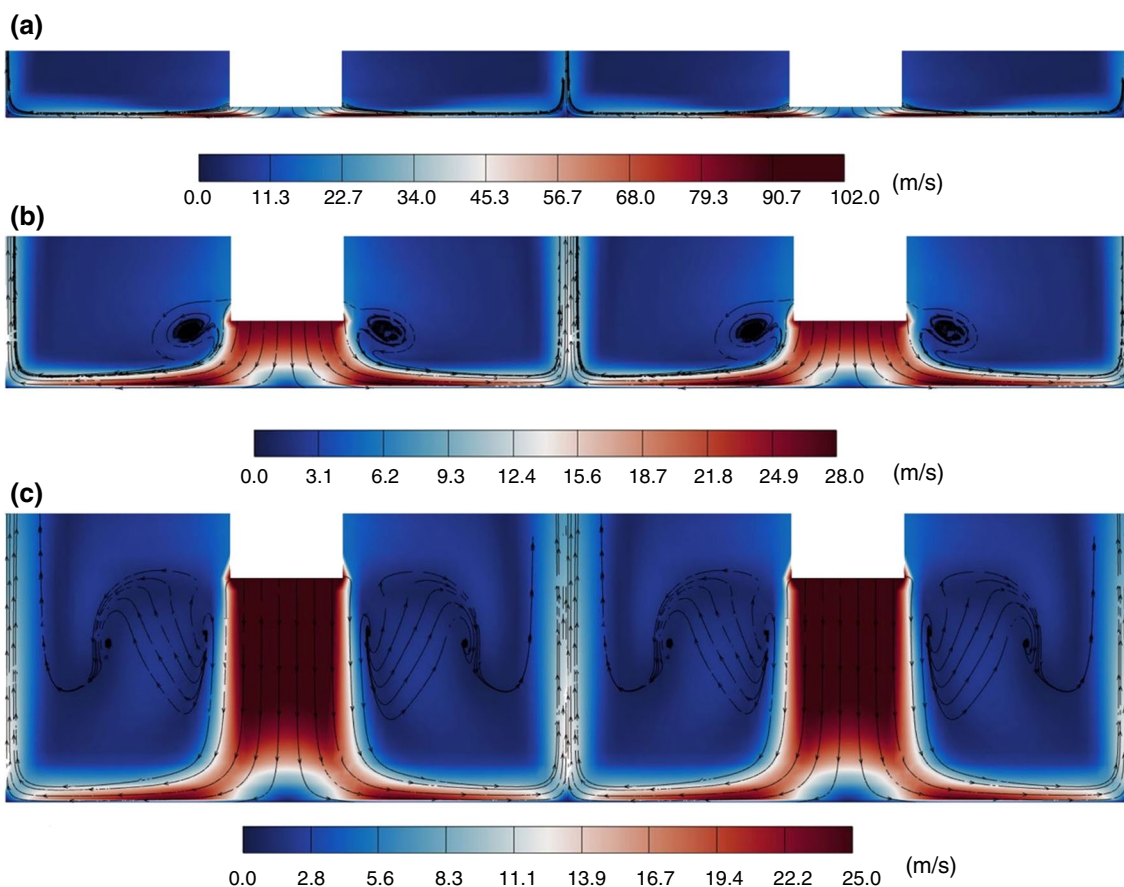Figure 11 shows the impact of jet-to-surface distance on the average Nusselt number along the z-direction for the low

Fig. 12 Effect of jet-to-plate distance on velocity distribution on the x–y plane at Re = 15,000 and dust concentration of 0.32 g m^{-3} for **a** H/D = 0.1; **b** H/D = 0.5; **c** H/D = 2

jet-to-surface distance. The mean Nusselt number along the z-direction can be calculated as follows:

$$\overline{Nu}(x) = \frac{1}{14D} \int_{-7D}^{7D} Nu(x,z)\mathrm{d}z \tag{15}$$

The results show that by reducing the jet-to-surface spacing, the Nusselt number increases. However, this increase is not significant for the jet-to-surface distance larger than 0.3.

Flow characteristics for dusty air

Figure 12 shows the effects of jet-to-target surface distance on the velocity distribution in the x–y plane. It can be observed that by decreasing the jet-to-plate distance, the velocity magnitude increases around the impingement region. Based on the results reported in this figure, by decreasing the jet-to-plate spacing from H/D = 0.5 to H/D = 0.1, the maximum velocity increases about 253% and 264% for the Reynolds number of 15,000, respectively. This significant increase in the velocity of the fluid increases the turbulent kinetic energy and leads to an increase in the heat transfer rate. The significant decrease in the velocity magnitude can be observed in the region between the jets for all jet-to-surface distances and Reynolds numbers. It should be noted that the velocity reduction between the jets (dead

fluid zone) consequences the decrease in heat transfer rate in this region.

Figure 13 shows the impact of jet-to-jet distance on the velocity distribution at different vertical sections, including X/P = 0.1, X/P = 0.2, X/P = 0.3, and X/P = 0.4. As shown in this figure, by reducing the jet-to-jet distance from P/D = 8 to P/D = 5, the value of velocity significantly increases. The considerable velocity increase in the near the wall can be observed for all values of X/P. It should be noted that the velocity increase in the near the wall leads to enhance the heat transfer rate at this region.

The effects of dust concentration on the average Nusselt number at P/D = 5 are presented in Table 2. In this table, the averaged Nusselt number for the various cases studied is calculated by Eq. 13. It can be found that at the same jet-to-surface spacing (H/D), the increase in jet Reynolds number leads to the enhancement of averaged Nusselt number for both clean and dusty air. Results in Table 2 reveal that for the jet Reynolds number of 7000, the air with the dust concentration of 1.8 gr m^3 provides a higher averaged Nusselt number by 18%, 45.8% and 39.5% times more than those for the clean air at the jet-to-surface distances of 0.1, 0.5 and 2, respectively.
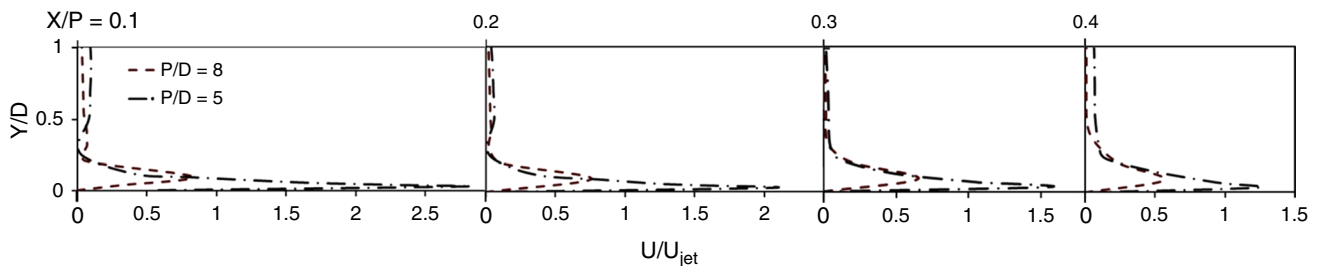

Fig. 13 Effect of jet-to-jet distance on velocity distribution at Re = 7000 and dust concentration of 0.32 g/m3 for **a** X/P = 0.1; **b** X/P = 0.2; **c** X/P = 0.3; **d** X/P = 0.4

Table 2 Effects of dust concentration on average Nusselt number for P/D = 5

Jet-to-surface distance	Re = 7000			Re = 15,000		
	H/D = 0.1	H/D = 0.5	H/D = 2	H/D = 0.1	H/D = 0.5	H/D = 2
Clean air	91.13	33.14	31.78	253.40	72.11	67.05
Dusty air with dust concentration of 0.32 g m^{-3}	99.31	39.84	36.70	270.69	83.93	76.92
Dusty air with dust concentration of 1.8 g m^{-3}	107.55	48.32	44.35	293.43	91.09	83.60

Conclusions

In the present study, the effects of dust concentration, jet-to-surface distance, and jet-to-jet distance on the flow velocity and Nusselt number distribution from a row impinging jets on the flat surface have been investigated. Constant heat flux of 2.0 kW·m^{-2} has been used on the flat surface. The predicted local Nusselt numbers by numerical simulation have been compared with the experimental data to benchmark the accuracy of the numerical method. The important results can be summarized as:

- By placing the nozzles at the low jet-to-target plate distance (e.g., H/D = 0.1), the Nusselt number in the region between the jets significantly decreases, while the value of Nusselt number in whole of the surface is considerably increased.
- Comparison between the experimental and numerical data confirms that the RNG k-ε turbulent model has the high ability to predict the Nusselt number.
- By using the nozzle-to-plate distance of H/D = 0.1, the average Nusselt number increases about 251.4% and 278.2% in comparison with the cases of H/D = 0.5 and H/D = 2, respectively.
- In the region between the jets, the average Nusselt number along z-direction for H/D = 0.1 is 2.03 and 2.46 times larger than those for the cases of H/D = 0.5 and H/D = 2.0, respectively, at Re = 15,000.
- The Nusselt number of dusty air is higher than that for the clean air in both stagnation and wall jet regions. The impinging air with dust concentration of 1.8 g m^{-3} increases the maximum Nusselt number by 18% in comparison with the clean air jet.
- For the jet the Reynolds number of 7,000, the air with dust concentration of 1.8 g m^{-3}, provides a higher averaged Nusselt number by 18%, 45.8% and 39.5% times more than the clean air for jet-to-surface spacing (H/D) of 0.1, 0.5 and 2, respectively.

Data Availability The data that support the findings of this study are available from the corresponding author upon reasonable request.

References

1. Esmailpour K, Bozorgmehr B, Hosseinalipour SM, Mujumdar AS. Entropy generation and second law analysis of pulsed impinging jet. Int J Numer Methods Heat Fluid Flow. 2015;25:1089–106.

2. Guo T, Rau MJ, Vlachos PP, Garimella SV. Axisymmetric wall jet development in confined jet impingement. Phys Fluids. 2017;29(2):025102.

3. Hadipour A, Rajabi Zargarabadi M, Mohammadpour J. Effects of a triangular guide rib on flow and heat transfer in a turbulent jet impingement on an asymmetric concave surface. Phys Fluids. 2020;32(7):075112.

4. Siddique MU, Syed A, Khan SA et al. On numerical investigation of heat transfer augmentation of flat target surface under impingement of steady air jet for varying heat flux boundary condition. J Therm Anal Calorim. 2021;1–13.

5. Doranehgard MH, Tran S, Dehghanpour H. Modeling of natural-gas diffusion in oil-saturated tight porous media. Fuel. 2021;300:120999.

6. Hadipour A, Zargarabadi MR, Dehghan M. Effect of micro-pin characteristics on flow and heat transfer by a circular jet impinging to the flat surface. J Therm Anal Calorim. 2020;140(3):943–51.

7. Lytle D, Webb BW. Air jet impingement heat transfer at low nozzle-plate spacings. Int J Heat Mass Transf. 1994;34:1687–97.

8. Norbert T, Abide S, Zeghmati B, Raminosoa C, Randriazanamparany MA. Numerical study of heat transfer and flow characteristics of air jet in a semi-confined cavity. Energy Procedia. 2018;139:682–8.

9. Singh P, Ekkad SV. Effects of spent air removal scheme on internal-side heat transfer in an impingement-effusion system at low jet-to-target plate spacing. Int J Heat Mass Transf. 2017;108:998–1010.

10. Grenson P, Léon O, Reulet P, Aupoix B. Investigation of an impinging heated jet for a small nozzle-to-plate distance and high Reynolds number: an extensive experimental approach. Int J Heat Mass Transf. 2016;102:801–15.

11. Glaspell AW, Rouse VJ, Friedrich BK, Choo K. Heat transfer and hydrodynamics of air assisted free water jet impingement at low nozzle-to-surface distances. Int J Heat Mass Transf. 2019;132:138–42.

12. Choo KS, Kim SJ. Heat transfer characteristics of impinging air jets under a fixed pumping power condition. Int J Heat Mass Transfer. 2010;53(1–3):320–6.

13. Choo K, Friedrich BK, Glaspell AW, Schilling KA. The influence of nozzle-to-plate spacing on heat transfer and fluid flow of submerged jet impingement Int. J Heat Mass Transf. 2016;97:66–9.

14. Greco CS, Paolillo G, Ianiro A, Cardone G, De Luca L. Effects of the stroke length and nozzle-to-plate distance on synthetic jet impingement heat transfer. Int J Heat Mass Transf. 2018;117:1019–31.

15. Zhu K, Yu P, Yuan N, Ding J. Transient heat transfer characteristics of array-jet impingement on high-temperature flat plate at low jet-to-plate distances. Int J Heat Mass Transf. 2018;127:413–25.

16. Hadipour A, Zargarabadi MR. Heat transfer and flow characteristics of impinging jet on a concave surface at small nozzle to surface distances. Appl Therm Eng. 2018;138:534–41.

17. Yu J, Peng L, Bu X, Shen X, Lin G, Bai L. Experimental investigation and correlation development of jet impingement heat transfer with two rows of aligned jet holes on an internal surface of a wing leading edge. Chin J Aeronaut. 2018;31(10):1962–72.

18. Fregeau M, Saeed F, Paraschivoiu I. Numerical heat transfer correlation for array of hot-air jets impinging on 3-dimensional concave surface. J Aircraft. 2005;42(3):665–70.

19. Craft TJ, Iacovides H, Mostafa NA. Modelling of three-dimensional jet array impingement and heat transfer on a concave surface. Int J Heat Fluid Flow. 2008;29(3):687–702.

20. Sharif MAR, Mothe KK. Parametric study of turbulent slot-jet impingement heat transfer from concave cylindrical surfaces. Int J Therm Sci. 2010;49(2):428–42.

21. Singh D, Premachandran B, Kohli S. Experimental and numerical investigation of jet impingement cooling of a circular cylinder. Int J Heat Mass Transf. 2013;60:672–88.

22. Fénot M, Dorignac E, Vullierme JJ. An experimental study on hot round jets impinging a concave surface. Int J Heat Fluid Flow. 2008;29(4):945–56.

23. Fénot M, Vullierme JJ, Dorignac E. Local heat transfer due to several configurations of circular air jets impinging on a flat plate with and without semi-confinement. Int J Therm Sci. 2005;44(7):665–75.

24. Whitaker SM, Peterson B, Miller AF, Bons, J.P. The effect of particle loading, size, and temperature on deposition in a vane leading edge impingement cooling geometry. ASME Paper No. 2016; GT2016–57413. 49798: V05BT16A013. (American Society of Mechanical Engineers).

25. Presley MA, Christensen PR. Thermal conductivity measurements of particulate materials 2 Results. J Geophys Res Planets. 1997;102(3):6551–66.

26. Zhang Y, Lou W, Liao M, Research on dust concentration measurement technique based on the theory of ultrasonic attenuation. In J. Phys. Conf. Ser. 2018; 986 (1): 012026. IOP Publishing.

27. Khoshvaght-Aliabadi M, Hassani SM, Mazloumi SH. Comparison of hydrothermal performance between plate fins and plate-pin fins subject to nanofluid-cooled corrugated miniature heat sinks. Microelectron Reliab. 2017;70:84–96.

28. Kline SJ. Describing uncertainty in single sample experiments. Mech Eng. 1953;75:3–8.

29. Yakhot VSASTBCG, Orszag SA, Thangam S, Gatski TB, Speziale C. Development of turbulence models for shear flows by a double expansion technique. J Phys Fluid. 1992;4(7):1510–20.

30. Bojdo N, Filippone A. A simple model to assess the role of dust composition and size on deposition in rotorcraft engines. Aerospace. 2019;6(4):44.

31. Patankar SV. Numerical Heat Transfer and Fluid Flow. Washington DC: Hemisphere; 1990.

32. Sproull WT. Effect of dust concentration upon the gas-flow capacity of a cyclonic collector. J Air Poll Cntl Assoc. 1966;16(8):439–41.

33. Krisak M. Environmental degradation of nickel-based superalloys due to Gypsiferous desert dusts. [Ph.D. Thesis]. Air Force Institute of Technology, 2015; WPAFB, OH, (USA).

34. Riaz A, Ellahi R, Sait SM. Role of hybrid nanoparticles in thermal performance of peristaltic flow of Eyring-Powell fluid model. J Therm Anal Calorim. 2021;143:1021–35.

35. Goodarzi M, Tlili I, Moria H, Alkanhal TA, Ellahi R, Anqi AE, Safaei MR. Boiling heat transfer characteristics of graphene oxide nanoplatelets nano-suspensions of water-perfluorohexane (C6F14) and water-n-pentane. Alexandria Eng J. 2020;59(6):4511–21.

36. Yin S, Li J, Shi G, Xue F, Wang L. Experiment study on heat transfer characteristics of dusty gas flowing through a granular bed with buried tubes. Appl Therm Eng. 2019;146:396–404.

37. Saber HH. Experimental characterization of reflective coating material for cool roofs in hot, humid and dusty climate. Energy Build. 2021;242:110993.

38. Khoshvaght-Aliabadi M, Sartipzadeh O, Pazdar S, Sahamiyan M. Experimental and parametric studies on a miniature heat sink with offset-strip pins and Al2O3/water nanofluids. Appl Therm Eng. 2017;111:1342–52.

39. Bozorg MV, Doranehgard MH, Hong K and Xiong Q, CFD study of heat transfer and fluid flow in a parabolic trough solar receiver with internal annular porous structure and synthetic oil–Al2O3 nanofluid. Renew Energy. 2020; 2598–2614.

40. Siavashi M, Karimi K, Xiong Q, Doranehgard MH. Numerical analysis of mixed convection of two-phase non-Newtonian nanofluid flow inside a partially porous square enclosure with a rotating cylinder. J Therm Anal Calorim. 2019;137(1):267–87.

41. Jia YU, Long PENG, Xueqin BU, Xiaobin SHEN, Guiping LIN, Lizhan BAI. Experimental investigation and correlation development of jet impingement heat transfer with two rows of aligned jet holes on an internal surface of a wing leading edge. Chin J Aeronaut. 2018;31(10):1962–72.